Liu *et al. Microplastics and Nanoplastics* (2026) 6:11
https://doi.org/10.1186/s43591-025-00170-5

Microplastics and Nanoplastics

RESEARCH Open Access

Functionalized polystyrene nanoplastics induce distinct toxicity and transcriptomic changes in human intestinal Caco-2 cells

Xueyan Liu[1†], Junbiao Wang[1†], Alessandra Borghi[1], Siyao Xiao[2], Giulio Caracciolo[2], Daniela Pozzi[2], Cristina Marchini[1*] and Cristina Miceli[1*]

Abstract

The plastic waste can be progressively disintegrated into microscale (MPs; 1 µm-5 mm) and nanoscale particles (NPs; 1 nm–1 µm) through the long-term influence of mechanical forces of water, ultraviolet radiation, and biological degradation. Humans are mainly exposed to MPs and NPs through oral intake. Following their ingestion, particles can penetrate intestinal mucosa, be transported to reach the circulatory system, and deposit in various organs, posing a serious risk to health. Polystyrene (PS) is an important thermoplastic found in disposable drinking cups, packaging, and personal care products. In the present study, unmodified PS or differently functionalized NPs (PS-COOH and PS-NH_2; 100 nm in size) were selected as experimental models and administered to colorectal adenocarcinoma Caco-2 cells, as a model of intestinal epithelia cells potentially highly exposed to microplastics. A comparison of internalization process into cells among differently functionalized NPs was performed by confocal microscopy and cytofluorimetric analysis. Fluorescent PS-COOH and PS-NH_2 NPs were detected to interact with cells after 2 h-incubation, and they continued to accumulate within 24 h. PS-NH_2 significantly reduced cell viability in a dose and time dependent way, while treatments with PS and PS-COOH were well tolerated and only the highest concentrations of PS-COOH were able to decrease cell viability after 96 h. From transcriptome sequence analysis 125 genes were differentially expressed by PS-NH_2 treatment for 24 h. Some genes were related to inflammation, apoptosis, and oxidative stress, and were involved in the Wnt signalling pathway. This study provides transcriptomic-level insights into the cellular responses of Caco-2 cells to PS nanoplastics, highlighting differentially expressed genes and pathways potentially associated with cytotoxicity.

†Xueyan Liu and Junbiao Wang contributed equally to this work.

*Correspondence:
Cristina Marchini
cristina.marchini@unicam.it
Cristina Miceli
cristina.miceli@unicam.it

Full list of author information is available at the end of the article

Graphical Abstract

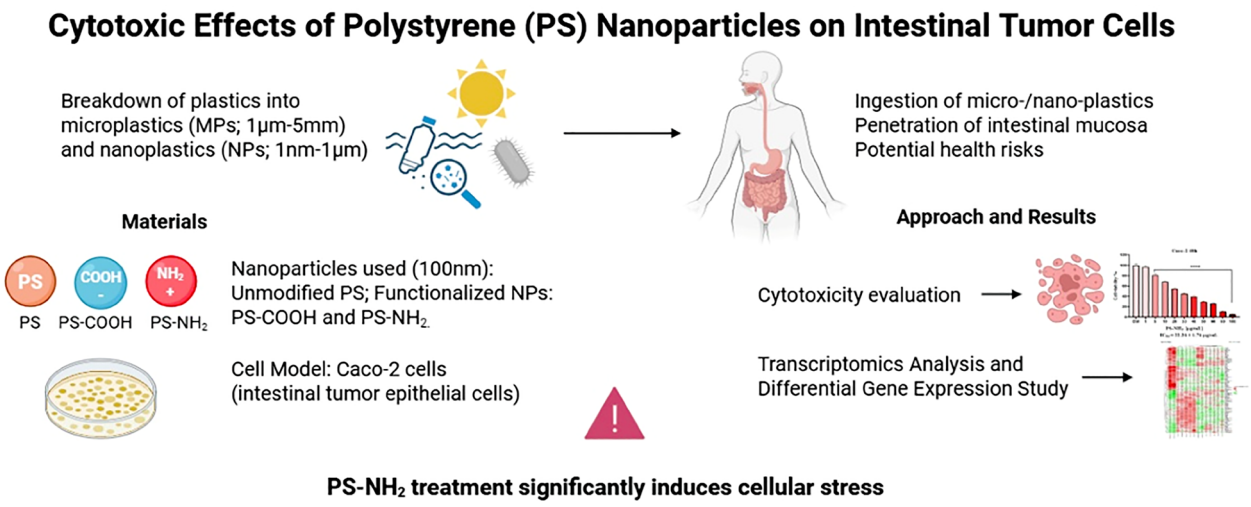

Keywords Nanoplastics, Human colon cells, Differential gene expression, Intestinal epithelial cells, Transcriptome analysis

Introduction

Plastics are ubiquitous in daily life and contribute significantly to environmental pollution, drawing growing scientific concern [1–4]. The term "microplastics" was first introduced by Thompson et al. to describe microscopic plastic debris representing persistent marine pollutants [5]. Microplastics (MPs) are commonly defined as plastic particles smaller than 5 mm and can be categorized in primary or secondary microplastics according to their source. MPs intentionally manufactured for commercial purposes, such as microbeads in facial scrubs and cosmetics and microfibers in textiles, are considered as primary MPs. Instead, secondary MPs describe small plastic fragments derived from the breakdown of larger plastic materials, such as water bottles and plastic bags, through physical, chemical, and/or biological processes [6, 7]. In particular, exposure to sunlight and ultraviolet (UV) radiation results in photo-degradation, oxidation and eventually plastics fragmentation [8, 9]. These secondary MPs have the potential to further degrade to nanoplastics (NPs), that are defined as particles with a size ranging between 1 nm and 1 µm and presenting a colloidal behaviour [10]. Due to their widespread distribution, MPs and NPs can enter the human body through ingestion of contaminated food and water, inhalation of NP-containing aerosols and via skin contact. NPs, due to their small size, can enter cells and trigger toxic effects, such as oxidative stress and growth inhibition [11–13]. MPs/NPs have been detected in human blood, lungs, reproductive organs, placenta, and feces [14–18], raising concerns about their health impacts. Ingestion is one of the major routes of human exposure to MPs/NPs. The intestine is thus a key target for plastic toxicity. After entering the digestive tract, particles can cross the intestinal mucosa, reach circulation, and accumulate in organs [19]. Although MPs consist of different plastic types with different sizes and shapes in nature, most of the studies on their biological impact have been done using plastic models with defined physicochemical characteristics, since heterogeneous composition and size distribution might interfere with reproducible results [20]. Considering that Polystyrene (PS) is among the most abundant MPs found in the environment, commercial PS beads are often used to mimic environmental microplastic particles and to evaluate their biological impact. PS is used in a variety of disposable items due to its low cost and ease of production [21, 22]. However, it is flammable, potentially releases harmful chemicals when heated, and is non-biodegradable. PS debris degrades into MPs/NPs and might undergo oxidation giving rise to functionalized forms like PS-COOH [23]. Surface charge plays a crucial role in toxicity; positively charged particles, such as PS-NH_2, can disrupt intestinal barrier function more than neutral or negatively charged ones [24]. PS MPs have been shown to alter gut microbiota and induce inflammation and metabolic disorders in animal models [25, 26]. Four-weeks PS NPs oral exposure in mice resulted in accumulation of NPs in liver, spleen, lung, kidney, intestine, testis, and brain, causing inflammation, and structure disorder in these tissues [27]. In vitro studies demonstrated that PS-MPs can be taken up by human epithelial colorectal adenocarcinoma (Caco-2) cells,

inducing redox and mitochondrial stress responses after 24 h of exposure [28]. Macropinocytosis and clathrin-mediated endocytosis were identified as the main routes for mediating uptake of PS NPs in intestinal cells, where their toxic effects are dependent on PS particles size and charge. Indeed, charged PS exhibited a stronger toxicity in comparison to pristine PS [27]. Although derived from colon carcinoma, Caco-2 cells differentiate into enterocyte-like cells, forming villi and expressing brush border enzymes [29–31], making them a widely accepted model for intestinal absorption studies. Marcellus et al. reported that after internalization PS MPs and NPs could be excreted by Caco-2 cells via exocytosis and they had no impact on barrier integrity when tested in differentiated mono- and tri-culture transwell models [32]. While MP and NP uptake is well documented and their health impacts of PS MPs/NPs are increasingly studied [33], only a few studies have analysed the effects of PS on human intestinal transcriptomic profiles. Among them, Wu et al. reported that Caco-2 cells exposed to PS MPs (5 µm) changed the transcription level of genes involved in proliferation (Ras, ERK, MER, CDK4, Cyclin D1) and inflammation (TRPV1, iNOS, IL-1β, IL-8) [34]. Although these studies have revealed inflammatory, oxidative, and metabolic effects [33], transcriptomic-level investigations of functionalized PS NPs in human intestinal cells remain limited, and further studies are needed to fully define the transcriptomic response of human cells to the exposure of plastic particles with different sizes and functionalization.

In this study, we investigated the transcriptomic response of human Caco-2 cells to PS, PS-COOH, or PS-NH_2 NPs (100 nm size) exposure, using RNA-seq, differential gene expression, gene ontology, and KEGG enrichment analyses, and the identified molecular pathways were correlated with PS NPs internalization properties and cytotoxicity. Our findings provide valuable transcriptomic insights into how PS NPs interact with intestinal epithelial cells, and unveil the global molecular response to PS NPs, advancing our understanding of their molecular toxicity and contributing to future risk assessments.

Methods

Nanoplastics characterization

Pristine polystyrene nanoplastics (NPs) (PS, 0.1 µm, non-fluorescent; Sigma, USA #43302) and fluorescently labelled functionalized polystyrene NPs (amino-modified polystyrene NPs (PS-NH_2, 0.1 µm, Sigma, USA #L9904) and carboxyl-modified polystyrene NPs (PS-COOH, 0.1 µm, Thermo Fisher, USA #5155) were spherical beads provided in aqueous solution. They were characterized, using 10 ug/mL NPs' concentration, by dynamic light scattering (DLS) and electrophoretic light scattering (ELS). Measurements were performed with a Zetasizer Nano ZS (Malvern Instruments Ltd., Malvern, UK), which allows determination of the hydrodynamic diameter and polydispersity index (PDI) by DLS, and zeta potential by ELS, as already described by Xiao et al. [35]. For size distribution, samples were analysed in disposable polystyrene cuvettes, whereas zeta potential measurements were carried out in folded capillary cells, following the manufacturer's instructions. All measurements were performed at 37 °C, and the obtained values were reported as mean of at least three independent determinations (see Table 1).

Cell culture

Caco-2 cells (ATCC, USA) were cultured in high-glucose Dulbecco's Modified Eagle Medium (DMEM; Gibco, USA) supplemented with 10% fetal bovine serum (FBS; Gibco, USA), 1% non-essential amino acids (Sigma, USA), and 1% penicillin–streptomycin (Corning, USA) at 37 °C in a humidified atmosphere containing 5% CO_2. Caco-2 cells were used at passage 38 and routinely tested to confirm the free of mycoplasma contamination. Cells were initially maintained in 25 cm^2 flasks and subsequently seeded into multi-well plates for experimental treatments. Cell growth was monitored daily and passaged at 80–90% confluence, to avoid differentiation in the cell monolayer. Experiments were performed in undifferentiated Caco-2 cells.

Cell viability assay

Caco-2 cells were seeded at 8,000 cells/well in 96-well plates using complete medium. After 24 h, cells were

Table 1 Hydrodynamic diameter, polydispersity index and zeta potential of pristine unmodified and functionalized amine-modified and carboxyl-modified systems. Values are reported as mean ± SD; $n = 3$

Sample	Dispersant	T (℃)	Z-Ave (d.nm)	SD	Polydispersity PDI	SD	ζ-potential (mV)	SD
PS	H_2O	37	126.67	4.04	0.02	0.02	-20.08	1.12
	DMEM		220.60	2.98	0.32	0.04	-15.90	1.31
PS-COOH	H_2O		129.20	6.46	0.02	0.01	-39.96	1.04
	DMEM		261.80	2.77	0.27	0.05	-14.80	1.72
PS-NH_2	H_2O		97.78	5.25	0.10	0.03	38.07	0.89
	DMEM		164.50	8.49	0.25	0.03	-14.05	0.59

exposed to PS, PS-COOH, or PS-NH_2 NPs (1–100 µg/mL) in DMEM containing 2% FBS for 24 h, 48 h, or 96 h. Untreated cells served as controls, and cell-free wells containing NPs were included as blanks to account for potential optical interference in the MTT [3-(4,5-dimethylthiazol-2-yl)-2,5-diphenyl-2 H-tetrazolium bromide Sigma Aldrich, St. Louis, MO] assay. Plates were washed with PBS before adding MTT. Cell viability was assessed using the MTT method as described by Xiao et al. [35]. Each condition was tested with 7 replicates, in three independent experiments. IC_{50} values were calculated by fitting the concentration–effect curve data obtained in the three experiments with the sigmoid-Emax model using nonlinear regression, weighted by the reciprocal of the square of the predicted effect.

Confocal microscopy

In a preliminary experiment, Caco-2 cells were seeded at 20,000 cells/well and exposed to fluorescently labelled PS-NH_2 (20 µg/mL) or PS-COOH (40 µg/mL) for 2 h, 4 h, 6 h, 8 h, or 24 h. Then, confocal microscopy analysis was repeated using the same exposure concentration for both PS-NH_2 or PS-COOH particles (10 µg/mL) to better compare their uptake by cells. This concentration was selected based on preliminary cytotoxicity data to ensure sub-cytotoxic yet biologically relevant exposure levels suitable for imaging. All samples were washed with PBS before confocal microscopy analysis, to remove unbound particles. Cell membranes were stained with 5 mg/mL Nile Red (Sial, Italy) and visualized using a Nikon Eclipse Ti confocal microscope (excitation 570 nm, emission 561 nm). Images were analysed using ImageJ Fiji (version 2.9.0), and at least five randomly selected fields were evaluated for each treatment [36].

Flow cytometry

Caco-2 cells were seeded at 5×10^5 cells per well in 6-well plates and, after 24 h, treated with 10 µg/mL PS-NH_2 or 10 µg/mL PS-COOH in DMEM containing 2% FBS for 4–24 h. All samples were washed with PBS before flow cytometry measurements, to remove unbound particles. Flow cytometric measurements were performed using a BD FACSCalibur (BD Life Sciences, San Jose, CA, USA; excitation 488 nm, emission 530/30 nm) equipped with CellQuest™ software, as described by Xiao et al. [35]. Each condition was tested in quadruplicate, in two independent experiments.

Total RNA extraction and transcriptome sequencing

Caco-2 cells were seeded at a density of 5×10^5 cells per well in a 6-well plate. The day after, cells were treated with 10 µg/mL PS, PS-NH_2 or PS-COOH in DMEM supplemented with 2% FBS, for 6–24 h. Total RNA extraction was performed by using EuroGold Trifast™ kit (Euroclone Company, Italy) according to the manufacturer's instructions and after washing with sterile PBS, and then store at -80 ℃ for subsequent sequencing and qRT-PCR analysis. RNA concentration and purity were determined using a Qubit fluorometer and a NanoDrop 2000 spectrophotometer (Thermo Fisher Scientific, Waltham, MA, USA). RNA integrity was evaluated with an Agilent 2200 TapeStation system (Agilent Technologies, Santa Clara, CA, USA). Some extractions were repeated because only samples with an RNA Integrity Number (RIN) greater than 7 were used for sequencing. A TapeStation report is shown in Supplementary Fig. 1. Qualified RNA samples were sent to BMR Genomics (Padova, Italy) for library preparation using the Illumina TruSeq Stranded mRNA Library Prep Kit and sequenced on an Illumina NextSeq 500 platform (75 bp paired-end reads). Reads quality was checked using the FastQC software [37]. Reads were deposited to NCBI Sequence Read Archive database, SRA accession: BioProject ID PRJNA1289666.

Transcriptome analysis

The clean reads, ranging from 21,909,573 to 31,893,244 as shown in Supplementary Table 1 (S-Table 1), were aligned to the human reference genome GRCh38 (release GRCh38.p13, accessed in February 2025) using Omics Box (BioBam informatics). Principal component analysis (PCA) was performed using gene expression data to show the differences in the gene expression profile of each group. Differentially expressed genes (DEGs) were identified using DESeq2 (v1.10.1) [38] with $|\log2FC| \geq 1$ and FDR < 0.05. Gene ontology (GO) terms were retrieved using PANTHER, and pathway enrichment analyses were performed with WebGestalt (version 2023, accessed in February 2025) [39].

Quantitative real-time PCR (qRT-PCR)

To confirm the results of transcriptome sequencing, 7 specific DEGs related to PS-NH_2 exposure responses were chosen for verification by qRT-PCR. The primer sequences and related information are shown in S-Table 2. PrimeScript RT Reagent Kit (Sial, Italy) was used for the cDNA synthesis. The qPCR analysis was performed as in Piersanti et al. [40], the analysis was run in triplicate. The relative expression level of each gene was normalized to the endogenous β- Actin gene since this gene has been found not significantly changed by PS treatments with respect to controls. Measurements of the β- Actin gene were repeated by qPCR and, again, significantly gene expression changes were not found between treatments and controls. All expression ratios were calculated using the $2^{-\Delta\Delta}$ Ct method.

Western blot

Caco-2 cells were seeded at a density of 5×10^5 cells per well in a 6-well plate. The day after, cells were treated with 10 µg/mL PS, PS-NH_2 or PS-COOH in DMEM supplemented with 2% FBS, for 48 h. The cells were lysed in RIPA buffer with protease inhibitors. Equal protein amounts were resolved by SDS-PAGE (Bio-Rad) and transferred to polyvinylidene difluoride (PVDF) membranes (Millipore). Membranes were then blocked with EveryBlot Blocking Buffer (Bio-Rad) and probed with primary antibodies against ERK (cat. #4695s) and p-ERK (cat. #4370s) (CellSignaling; 1:1000), and β-actin (sc-47778, lot #K1607; Santa Cruz). Secondary HRP-conjugated antibodies (Sigma) were detected with ECL substrate (Thermo Scientific) using ChemiDoc™ XRS-System (Bio-Rad). Densitometry analysis was performed through ImageJ software (Version: 2.1.0/1.53 C).

Statistical analysis

Figures and statistical analyses were performed using GraphPad Prism 10.6 (GraphPad Software, San Diego, CA, USA). Data were tested for normality using the Shapiro–Wilk test. When assumptions of normality or homogeneity of variance were met, one-way ANOVA was applied for multiple-group comparisons, followed by Dunnett's or Tukey's post hoc tests as indicated in the figure captions. If assumptions were not satisfied, the non-parametric Kruskal–Wallis test was used instead. Data are presented as means ± standard error of the mean (SEM). RNA-sequencing data were analysed in R (version 4.0.3) using Student's *t*-test, with statistical significance determined at a false discovery rate (FDR)-adjusted $p < 0.05$. Venn diagrams were generated using the VennDiagram package, and other visualizations were produced with ggplot2 in R.

Results

Nanoplastics characterization

Pristine polystyrene nanoplastics (NPs) (PS), amino-modified polystyrene NPs (PS-NH_2) and carboxyl-modified polystyrene NPs (PS-COOH) were characterized by dynamic light scattering (DLS) and electrophoretic light scattering (ELS) to determine their hydrodynamic diameter, polydispersity index (PDI) as well as their zeta potential. Measurements were performed both in water and in culture medium (DMEM) at 37 °C and the obtained values were reported in Table 1.

When measurements were performed in H_2O, DLS showed that PS-COOH NPs had a mean hydrodynamic diameter of 129.2 ± 6.46 nm with a low polydispersity index (PDI = 0.02), while PS-NH_2 were slightly smaller (97.78 ± 5.25 nm) and exhibited a broader size distribution (PDI = 0.10). Zeta potential measurements confirmed the expected opposite surface charges: PS-COOH displayed a strong negative charge (−39.96 ± 1.04 mV), whereas PS-NH_2 carried a high positive charge (+ 38.07 ± 0.89 mV). Unmodified PS particles had a hydrodynamic size of 126,67 ± 4.04 nm with a PDI of 0.02 and exhibited a negative zeta potential around − 20.08 mV. Thus, the employed particles were monodispersed (uniform) nano-scale objects in water, with a different surface charge. However, when measurements were performed in cell culture medium (DMEM), their hydrodynamic size and PDI increased, while their absolute ζ-potentials decreased towards the ζ-potential of DMEM (~ -17.81 mV), suggesting the adsorption of small medium components (Table 1).

In agreement with previous observations on colloidal systems in cellular media [41], PS-NH_2 NPs exhibit a marked reduction of surface charge and even a shift to negative ζ-potential values when dispersed in DMEM. This effect is expected, as DMEM contains a high concentration of inorganic anions (e.g., phosphate, bicarbonate, chloride) that readily adsorb onto positively charged surfaces through electrostatic interactions. Such anion binding is generally weak and reversible and does not imply the formation of a stable coating. Rather, it reflects a rapid ionic screening process that modifies the electrokinetic potential measured at the slipping plane, while leaving the underlying surface chemistry of the particles unchanged. For this reason, charge reversal in DMEM does not prevent PS-NH_2 NPs from interacting with cell membranes through charge-mediated, nonspecific processes once they approach the cell surface. Upon contact with the negatively charged glycocalyx and membrane proteoglycans, the loosely bound inorganic ions can be displaced, restoring the functional cationic interactions known to promote cellular association and uptake. This interpretation is consistent with established evidence showing that ionic components of biological and cell-culture media can transiently alter nanoparticle ζ-potential without abolishing their intrinsic charge-dependent biological behaviour.

PS NPs cytotoxicity analysis

To assess the toxicity of functionalized PS nanoparticles (characterization methods are described in the Methods section), Caco-2 cells were exposed to amino-modified PS-NH_2, carboxyl-modified PS-COOH, and unmodified PS nanoparticles at concentrations ranging from 1 to 100 µg/mL for 24, 48, and 96 h, respectively. MTT assays showed that PS-NH_2 significantly reduced cell viability in a dose- and time-dependent manner, with an IC_{50} of approximately 43 µg/mL at 24 h, 22 µg/mL at 48 h, and 5 µg/mL at 96 h. In contrast, PS-COOH only reduced cell viability after 96 h of culture at a concentration of 100 µg/mL, while unmodified PS showed no toxic effect (Fig. 1).

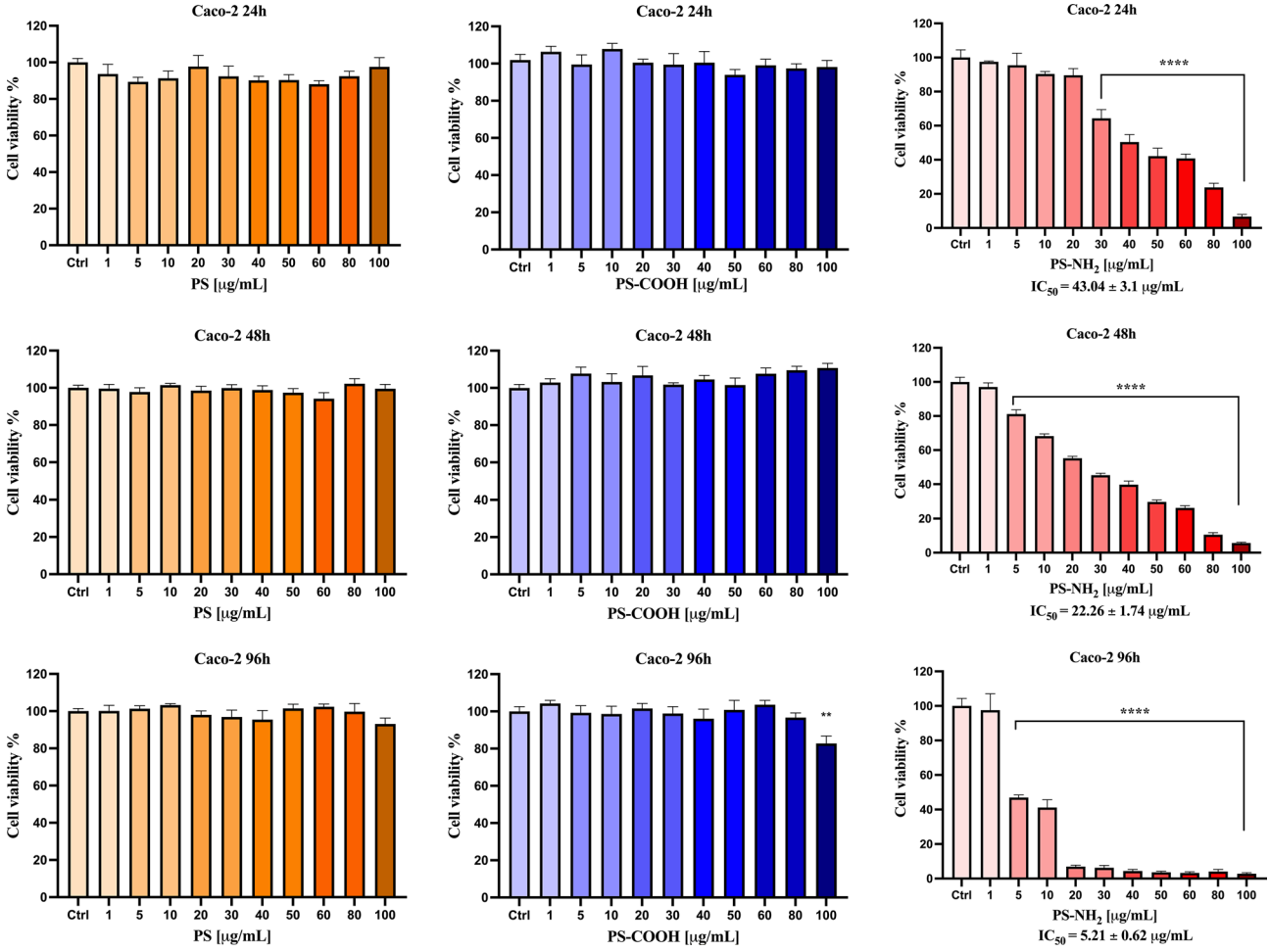

Fig. 1 Effect of 100 nm PS NPs on Caco-2 cell viability. Caco-2 cells were untreated (control) or exposed for 24, 48, or 96 h to increasing concentrations of PS (left panels; orange), PS-COOH (middle panels; blue), or PS-NH_2 (right panels; pink). Cell viability was determined by MTT assay. Columns represent means of three independent experiments; data are presented as means ± SEM ($n = 7$). Statistical analysis was performed using one-way ANOVA followed by Dunnett's post hoc test. p-values indicate comparisons versus the control group: $^{**}p < 0.01$, $^{****}p < 0.0001$

Study of functionalized PS NPs interaction with Caco-2 cells

In a preliminary experiment, Caco-2 cells were incubated with fluorescently labelled PS-NH_2 (20 μg/mL) and PS-COOH (40 μg/mL), to analyse PS NPs interaction with intestinal cells by confocal microscopy. Fluorescent functionalized polystyrene PS-NH_2 and PS-COOH were detected interacting with Caco-2 cells after 2 h-incubation, and continued to accumulate within 24 h, as observed by confocal microscopy (S-Fig. 2). To compare the uptake of PS-NH_2 and PS-COOH by Caco-2 cells, the confocal microscopy analysis was repeated using the same exposure concentration for both PS-NH_2 and PS-COOH particles (10 μg/mL). To determine whether NPs penetrate cells or merely associate with the plasma membrane, Nile Red, a lipid-specific dye labelling both the membrane and internal vesicles, was used.

The green-fluorescent signal indicated that PS-NH_2 mainly localized at the red-stained cell membrane since only a limited number of green spots were visible inside the cells, and they appear yellow in the merged images to indicate their localization in membrane compartments (Fig. 2A, PS-NH_2: merged and middle section). Conversely, PS-COOH entered in larger amount inside cells, also in membrane compartments, as shown by the numerous yellow spots in the merge image in Fig. 2A (PS-COOH: merged and middle section images). These preferential localizations of the two types of charged PS were also confirmed by the profile of the detected fluorescence in the panels on the right of Fig. 2A. Orthogonal views are shown in supplementary materials (S-Fig. 3), as additional indication of the cellular localizations of the charged PS.

Flow cytometry experiments quantified PS NP-cell interactions and revealed that the fluorescence signal detected after 24 h incubation with both PS-NH_2 and PS-COOH was significantly higher than that measured after 4 h, suggesting a continuous accumulation of PS

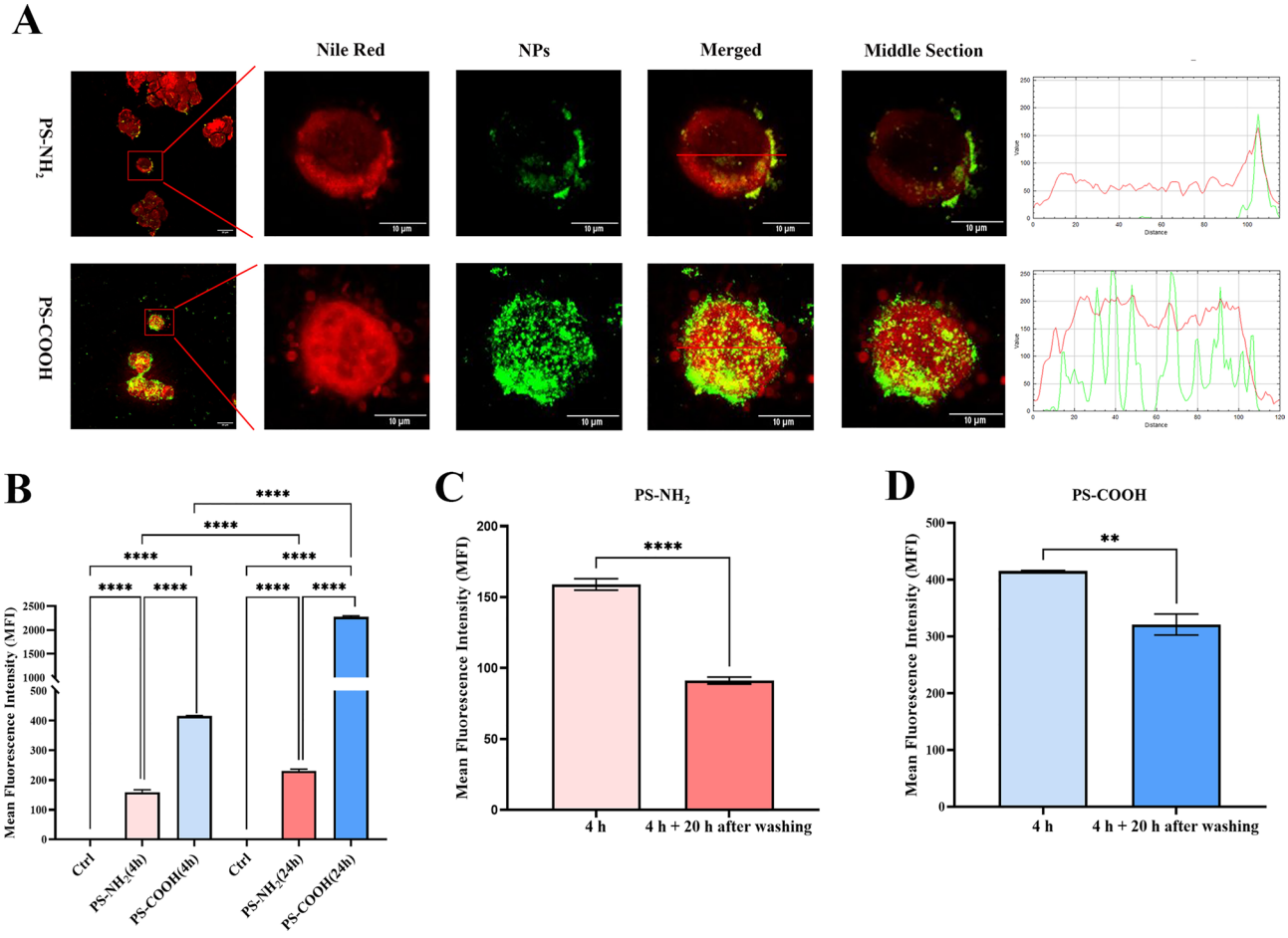

Fig. 2 Cellular association and localization of PS-NH_2 and PS-COOH NPs in Caco-2 cells. (**A**) Confocal images of cells treated with green-fluorescent PS-COOH (10 µg/mL) or PS-NH_2 (10 µg/mL) for 24 h and stained by Nile Red. On the right, Fluorescence intensity profile graphs (taken along the red line shown in merged section) with intensity of NPs in green and of Nile Red in red. Scale bars: 10 µm. (**B**) Flow cytometry quantification of mean fluorescence intensity of Caco-2 cells treated with PS-NH_2 (10 µg/mL) or PS-COOH (10 µg/mL) NPs for 4 h and 24 h. (**C**, **D**) FACS analysis after 4 h exposure and 20 h post-washing to assess NP retention. Data: mean ± SEM ($n = 4$, two experiments). Statistical analysis was performed using one-way ANOVA followed by Dunnett's post hoc test. $^{**}p < 0.01$; $^{****}p < 0.0001$ (unpaired Student's t-test)

NPs in Caco-2 cells during the monitored time. Moreover, a stronger fluorescent signal was detected for PS-COOH compared to PS-NH_2 treated cells both after 4 h and 24 h exposure (Fig. 2B). To evaluate if Caco-2 cells release PS NPs, they were washed after 4-hour exposure with PS-NH_2 or PS-COOH, and left untreated for additional 20 h, when fluorescence signal was again acquired. Washed cells remained fluorescent, although a reduction in the signal intensity was observed with respect to cells exposed for 4 h (Fig. 2C, D). While PS-NH_2 treated cells retained 57.38% of the nanoparticles, PS-COOH treatment showed a reduction of 22.65% in cell-associated NPs after washing. This decrease may reflect detachment from the cell surface or exocytosis, as previously observed in similar intestinal epithelial models treated with smaller pristine PS nanoparticles [42].

Transcriptomic profile and differentially expressed genes in Caco-2 cells in response to pristine and functionalized PS NPs treatments

To investigate the distinct effects of PS-NPs exposure on the gene expression profile of Caco-2 cells, we incubated the cells with pristine PS, PS-NH_2, and PS-COOH for 6 h and 24 h at a sub-lethal concentration of 10 µg/mL.

After mapping the sequencing reads to the human genome, we performed PCA that showed the clustering of samples according to the duration of exposure (Fig. 3A). In the 6-hour exposure cluster, samples treated with pristine PS or with PS-COOH appeared more homogeneous and closely overlapped with control samples, suggesting no evident effect of these treatments on the transcriptomic profile. In contrast, PS-NH_2-treated samples clustered separately. A similar pattern, with more distinct sample separation, was observed in the 24-hour exposure cluster.

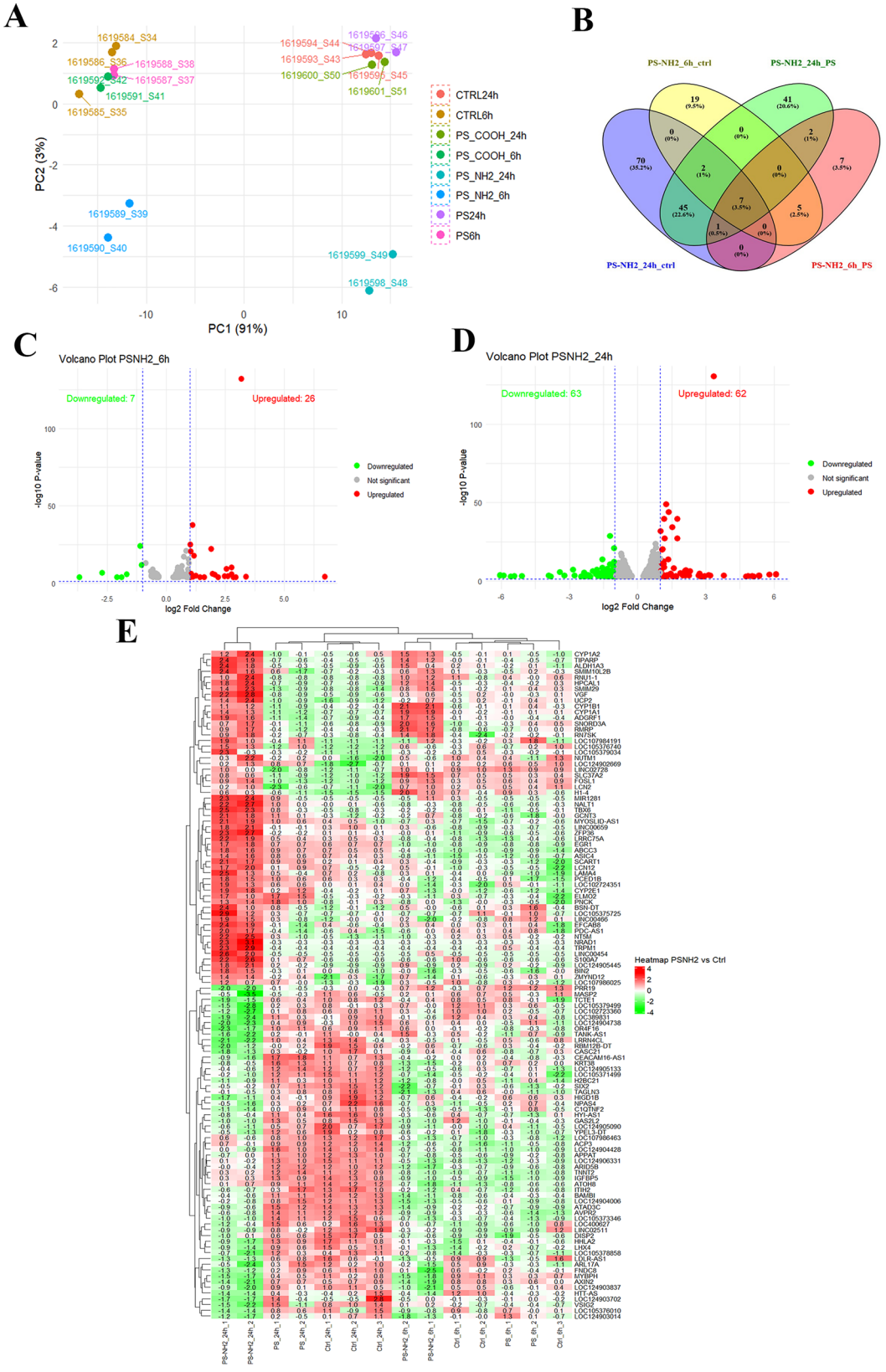

Fig. 3 Differentially expressed genes (DEGs) under nanoplastic exposure. (**A**) PCA of gene expression in Caco-2 cells treated with PS, PS-NH_2, PS-COOH, or left untreated (control; CTRL) at different time points. (**B**) Venn diagram of DEGs from PS-NH_2 (6 h and 24 h) vs. CTRL and PS. (**C**, **D**) Volcano plots of DEGs in PS-NH_2 at 6 h and 24 h vs. CTRL. (**E**) Heatmap of DEGs from PS-NH_2 (24 h), with expression levels in CTRL and PS groups at 6 h and 24 h. Values are represented by a range of colours from red (highly expressed) to green (lowly expressed)

Table 2 Common 7 DEGs for treatments relative to controls

Gene name	Dysregulation	Gene annotation
RMRP	Upregulated	RNA Component of Mitochondrial RNA Processing Endoribonuclease
CYP1B1	Upregulated	Cytochrome P450 1B1
CYP1A1	Upregulated	Cytochrome P450 1A1
ADGRF1	Upregulated	Adhesion G Protein-Coupled Receptor F1
RN7SK	Upregulated	RNA Component Of 7SK Nuclear Ribonucleoprotein
AXIN2	Downregulated	Axis inhibition protein 2
KRT38	Downregulated	Keratin 38

DEG identification was conducted by comparing treated samples with controls and by comparing samples treated with functionalized PS NPs to those treated with pristine PS. No significant DEGs were identified at either exposure time when comparing treatments with pristine PS to controls, PS-COOH to controls, or PS-COOH to pristine PS.

Conversely, exposure to PS-NH_2 for 6 h compared to controls resulted in 33 DEGs, comprising 26 upregulated and 7 downregulated genes (Fig. 3C). Exposure to PS-NH_2 for 24 h compared to controls yielded 125 DEGs, with 62 upregulated and 63 downregulated genes (Fig. 3D).

Despite the minimal differences observed between pristine PS treatment and controls, we also compared the results of PS-NH_2 treatment to those of pristine PS treatment at both exposure times. The DEGs identified by comparing PS-NH_2 treatment to controls provide a general indication of the cellular response; however, DEGs also dysregulated in the comparison between PS-NH_2 and pristine PS treatments may be associated with the additional charged group on the nanoplastics.

As shown in the Venn diagram (Fig. 3B), analysis of DEGs from comparisons of PS-NH_2 treatments with controls and with pristine PS treatments at both time points revealed 55 shared DEGs, likely affected primarily by the specifically positively charged polystyrene nanoparticles. Among these 55 DEGs, seven are shared across both exposure times and are listed in Table 2, indicating time-independent expression. For a visualization of the degree of gene dysregulation detected by the comparisons of the PS-NH_2 and PS treatments with controls at 6 h and 24 h, an extended heatmap with gene names is reported in Fig. 3E.

Functional annotation and classification of the DEGs

To investigate the biological importance of the DEGs, GO functional enrichment analysis was performed. Both 6 h and 24 h PS-NH_2 treatment displayed a similar GOs pattern (Fig. 4A and B). In the biological process category, cellular process, biological regulation and developmental process were the dominant functional terms. Cellular anatomical entity and protein-containing complexes were the top functional terms in the cellular component category. Most of the DEGs in the category of molecular function were related to binding, catalytic activity, and transcription regulator activity.

It is evident that PS-NH_2 treatment, at different times of exposure influences the same processes, although different genes are activated during time and the number

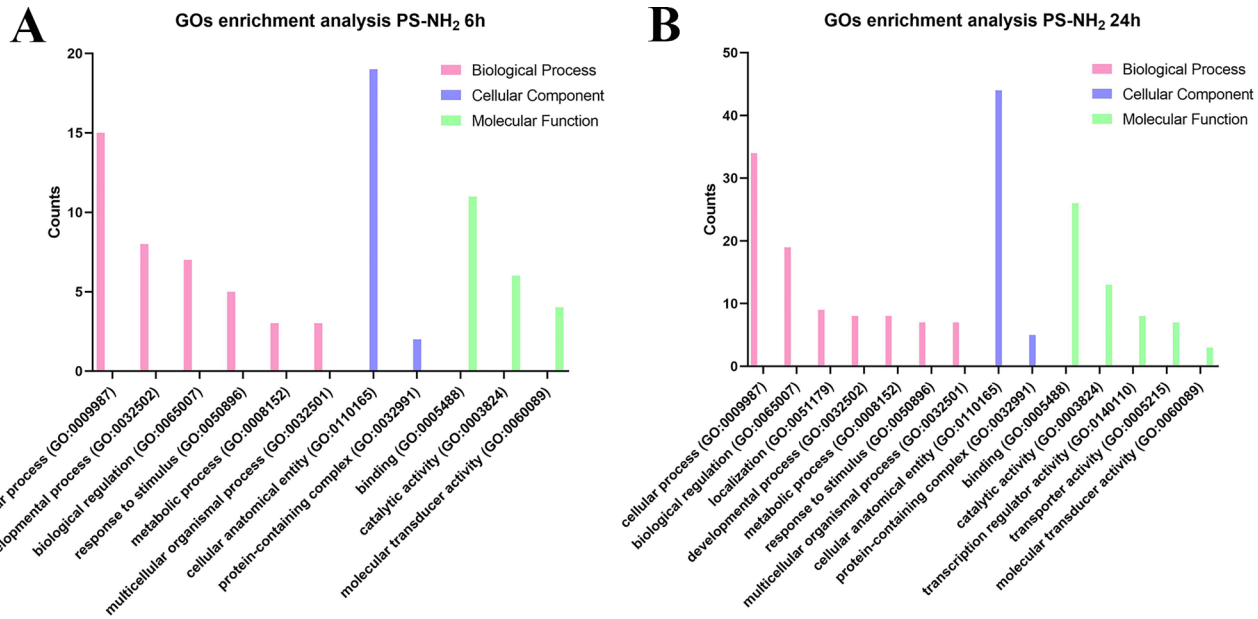

Fig. 4 GO classification of DEGs in PS-NH_2-treated cells. (**A**) 6 h and (**B**) 24 h exposure groups. BP: biological process; CC: cellular component; MF: molecular function. Only terms involving multiple genes are shown

of involved genes increases at the longer exposure. We focused our attention on the GOs term Localization (GO: 0051179) where dysregulation of genes as *KCNE5*, *ASIC4* and *ABCC3* suggest an impact on the membrane, especially involving the type of ions and substances that can pass (S-Table 3). Nonetheless, the genes involved in molecular transport shown in S-Table 3, are shared between of PS-NH_2 24 h treatment compared with controls and with PS treatment, suggesting an effect related to the positive charge of PS-NPs.

In addition, S-Table 4 reports DEGs that may be involved in different biological processes affected by the PS-NH_2 cell interaction, as later discussed.

Cytochrome p450 and Wnt pathway involvement in PS-NH_2 response

The analysis of the DEGs of the condition PS-NH_2 compared to controls was also done with Web Gestalt to identify which of the known KEGG pathways were involved. We used the multi-omics option, considering the temporality of the stressor rather than analysing the 6 h and 24 h separately. As a result, we identified 4 pathways in the KEGG database (Table 3, upper part), including Chemical carcinogenesis and Metabolism of xenobiotics by cytochrome P450. These findings highlight the critical role of cytochrome P450 in the cellular response to environmental stressors.

Among all the cytochrome genes overexpressed, *CYP1A1* was common in both conditions. *CYP1A1* and *CYP1B1* are encoding well-studied cytochrome p450 enzymes that are classically known to metabolize xenobiotic chemicals. In addition, the gene aldehyde dehydrogenase 3 family member A1 (*ALDH3A1*), that is also involved in the cytochrome pathway is upregulated [43]. Finally, the up- regulation of additional members of the cytochrome family, like *CYP2E1*, suggests the presence of reactive oxygen species in the cell, and indicate the inflammation the cell is going throw.

Regarding the comparison between the treatments with PS-NH_2 and with pristine PS, by KEGG analysis, similar GOs pathways were found (Table 3, bottom part), and specifically the Wnt signalling pathway appeared statistically significantly affected. In the PS-NH_2 treatment compared to controls, genes like *AXIN2*, *BAMBI*, *FOSL-1*, known to be part of the Wnt pathway were found dysregulated as shown in the heatmap (Fig. 3E). The canonical Wnt/β-catenin signalling pathway is recognized as a driver of colon cancer and one of the most representative signalling pathways. Dysregulation of the degradation of β -catenin, the functional effector molecule of the Wnt pathway, is in fact representative of the development and the progression of colon cancer [44].

The overexpression of *FOSL1* (a transcription factor from the activator protein-1 (AP-1) superfamily) in Caco-2 cells exposed to PS-NH_2 can be the consequence of an increased expression of β-catenin or *TWIST*, since both transcription factors are able to bind to its promoter [45]. However, *FOSL1* can be also induced by MAPK (mitogen-activated protein kinase) activation [46]. Thus, to investigate the involvement of the MAPK signalling pathway in *FOSL1* overexpression, we analysed by western blot the expression level of ERK and phosphorylated ERK (activated ERK form) in Caco-2 cells exposed to PS, PS-NH_2 and PS-COOH. Treatment of Caco-2 cells with 10 μg/mL PS-NH_2 resulted in a marked decrease in phosphorylated ERK, indicating a strong downregulation of the MAPK signalling pathway. A similar effect was obtained only with 10-fold higher concentrations (100 μg/mL) of PS or PS-COOH. Therefore, PS and PS-COOH caused a weaker MAPK inhibition with respect to PS-NH_2 (S-Fig. 4). These results led us to exclude the hypothesis that *FOSL1* overexpression was related to MAPK pathway in PS-NH_2-treated Caco-2 cells.

Table 3 KEGG enrichment: PS-NH_2 vs. control, PS vs. PS-NH_2

Condition	Gene set	Description	Size	Genes involved	Meta-*p*	Meta FDR
PS-NH_2 24 h vs. controls	hsa00980	Metabolism of xenobiotics by cytochrome P450	78	*ALDH3A1*, *CYP1A1*, *CYP1A2*, *CYP1B1*, *CYP2E1*	8.2799e-7	0.00029476
	hsa00140	Steroid hormone biosynthesis	62	*CYP1A1*, *CYP1A2*, *CYP1B1*, *CYP2E1*	2.7989e-6	0.00049821
	hsa05204	Chemical carcinogenesis	70	*CYP1A1*, *CYP1A2*, *CYP1B1*, *CYP2E1*	5.4496e-6	0.00056670
	hsa00380	Tryptophan metabolism	42	*CYP1A1*, *CYP1A2*, *CYP1B1*	6.3674e-6	0.00056670
PS-NH_2 24 h vs. to PS	hsa00380	Tryptophan metabolism	42	*CYP1A1*, *CYP1A2*, *CYP1B1*	9.9290e-7	0.00035347
	hsa00140	Steroid hormone biosynthesis	62	*CYP1A1*, *CYP1A2*, *CYP1B1*	6.3145e-6	0.0011240
	hsa05204	Chemical carcinogenesis	70	*CYP1A1*, *CYP1A2*, *CYP1B1*	5.4496e-6	0.00056670
	hsa05207		212	*ADRB2*, *CYP1A1*, *CYP1A2*, *CYP1B1*, *FGF8*	1.4323e-5	0.0012747
	hsa00980	Metabolism of xenobiotics by cytochrome P450	78	*CYP1A1*, *CYP1A2*, *CYP1B1*	1.8461e-5	0.0013144
	hsa04913	Ovarian steroidogenesis	51	*CYP1A1*, *CYP1B1*	5.8765e-5	0.0034867
	hsa00830	Retinol metabolism	68	*ALDH1A3*, *CYP1A1*, *CYP1A2*	4.8477e-4	0.024654
	hsa04310	Wnt signalling pathway	174	*AXIN2*, *DKK4*, *FOSL-1*	6.8684e-4	0.030564

Moreover, considering the crucial role of the MAPK pathway in regulating cell proliferation and survival, its strong downregulation by PS-NH_2 might explain the higher survival rate of Caco-2 cells treated with PS and PS-COOH with respect to cells treated with PS-NH_2, as already reported in breast cancer cells by Xiao et al. [35].

Validation of the transcriptomic sequencing results by qRT-PCR

To validate the transcriptomic data, 7 genes dysregulated after 24 h PS-NH_2 exposure (*BAMBI*, *ADAMTS14*, *AXIN2*, *ZFP36*, *ADGRF1*, *ARRDC4*, and *FOSL1*) were analysed by qRT-PCR. Expression patterns matched RNA-seq results (Pearson R^2 = 0.9074; 95% CI: 0.7060 to 0.9932) (Fig. 5) indicating data reliability.

Discussion

NPs have been detected in multiple human tissues, including blood, lung, placenta, reproductive organs, and feces [14–18], raising concerns about their potential impact on human health. In this context, we investigated the effects of differentially charged PS-NPs on human intestinal epithelial Caco-2 cells to evaluate toxicity and transcriptional responses. Commercially available PS microspheres provide a chemically well-defined and reproducible model for studying the biological effects of micro- and nanoplastics; however, they do not fully capture the diversity, surface weathering, or compositional complexity of environmental particles. Future research using environmentally aged or field-collected micro- and nanoplastics is therefore needed for more realistic exposure assessments.

In this study, Caco-2 cells were used before reaching full confluence, a stage in which they have not yet undergone the differentiation process that produces tight junctions and enterocyte-like characteristics. Although differentiated monolayers are more physiologically representative of the intestinal barrier [47], non-differentiated Caco-2 cells provide important advantages for transcriptomic screening. Their more uniform and proliferative state reduces baseline heterogeneity, enabling treatment-induced transcriptional changes to be detected with greater sensitivity. Moreover, because junctional and barrier-related pathways become fully established only after polarization [47], early stress, xenobiotic, and signalling responses are less likely to be masked by strong homeostatic feedback typical of differentiated cells. Proteomic profiling further shows that differentiation involves upregulation of adhesion and tight-junction proteins and downregulation of proliferation markers [48]. Thus, differentiated cells are more suitable for host–microbiome interaction studies, which are not the focus of this work. Conversely, non-differentiated Caco-2 cells offer a useful model for a first mechanistic exploration, as also demonstrated in transcriptomic analyses performed under titanium dioxide exposure [49]. Follow-up studies in more complex systems, such as organoids, will nonetheless be required to confirm physiological relevance.

Using confocal microscopy and flow cytometry, we observed that both PS-COOH and PS-NH_2 NPs rapidly interact with Caco-2 cells. PS-COOH NPs were extensively internalized, likely through endocytic pathways, whereas PS-NH_2 NPs remained primarily associated with the cell membrane. Notably, PS-NH_2 exposure induced a significant, dose- and time-dependent loss of viability, while PS and PS-COOH induced minimal cytotoxic effects. These findings align with the physicochemical characterization: although both functionalized NPs retained nanometric size with acceptable monodispersity, their distinct surface chemistries resulted in contrasting electrostatic properties. The strong cationic charge of PS-NH_2 likely increases interactions with cellular

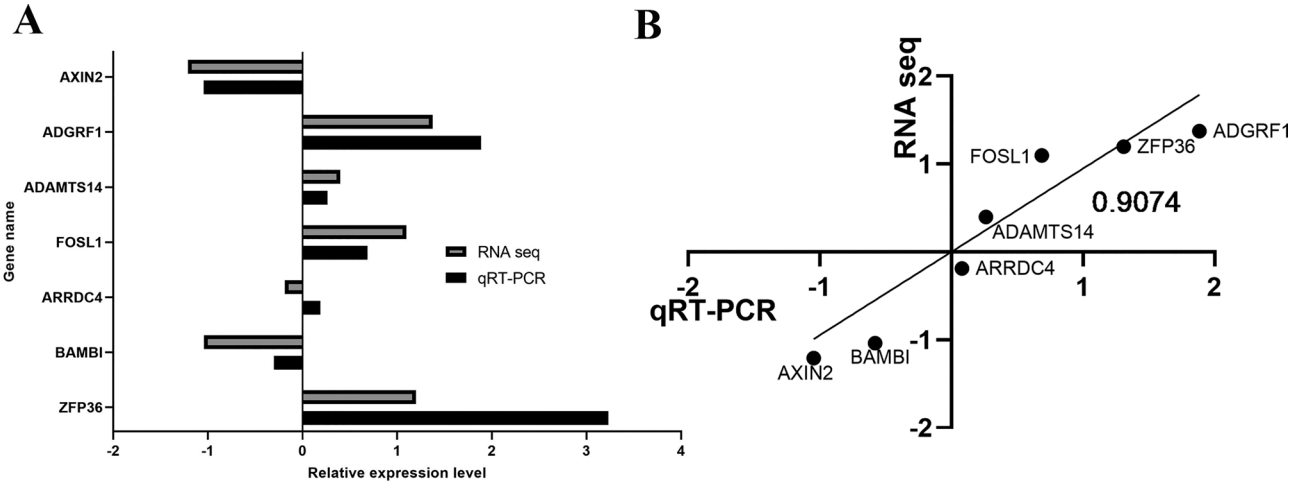

Fig. 5 Verification of the selected DEGs identified. (**A**) Expression levels of DEGs from RNA-Seq (fold change) and qRT-PCR ($2^{-\triangle\triangle}$ct); (**B**) Correlation between RNA-Seq and qRT-PCR of DEGs

membranes but also contributes to their higher cytotoxicity, in contrast to the negatively charged and comparatively biocompatible PS-COOH. These observations are consistent with previous studies identifying surface charge as a major determinant of NP toxicity [50–52].

The concentration-dependent cytotoxicity observed for PS-COOH and PS-NH_2 is consistent with earlier work showing that surface charge and exposure duration critically modulate nanoplastic toxicity in intestinal models [53]. The stronger adverse effects of positively charged PS-NH_2 align with their higher affinity for negatively charged membranes and their ability to disrupt epithelial integrity [54]. The reduced levels of cell-associated PS-COOH particles after washing, as shown in Fig. 2D, may reflect detachment from the membrane or active exocytosis. Similar behaviour has been reported in intestinal epithelial models, where functionalized or smaller PS nanoparticles were shown to undergo partial clearance over time [42, 55]. Although flow cytometry cannot distinguish internalized from membrane-bound particles, these findings, together with confocal observations, indicate that NP–cell interaction dynamics depend on surface charge and likely involve both membrane association and intracellular trafficking. They also reinforce the relevance of surface functionalization as a determinant of NP–cell interactions and, consequently, of distinct transcriptional responses.

Transcriptomic analysis following PS-NH_2 exposure revealed 33 DEGs at 6 h and 125 DEGs at 24 h, with only nine genes overlapping. Common DEGs included *CYP1A1* and *CYP1B1*, which were upregulated and encode heme-containing monooxygenases involved in xenobiotic metabolism [44, 56]. The gene encoding AXIN2, a key negative regulator of Wnt/β-catenin signalling [45, 57], was downregulated, as was *Rn7SK*, a small nuclear non-coding RNA that controls RNA Polymerase II transcription and has been implicated in apoptotic pathways [46, 58]. Consistently, GO analysis indicated involvement of inflammation, oxidative stress, apoptosis, and xenobiotic response.

The upregulation of CYP1A1 and CYP1B1, known inducers of ROS, suggests activation of detoxification and oxidative stress pathways, similar to responses observed under titanium dioxide exposure [49]. GBP3, significantly upregulated at 6 h, is a well-known mediator of inflammasome activation and innate immunity [59], reinforcing the immune-related transcriptional response. Additional upregulated genes involved in intracellular signalling included *FOSL1*, *ADGRF1*, *TWIST1*, and *ZFP36*, while *AXIN2*, *ARRDC4*, and *BAMBI* were consistently downregulated. Selected expression changes were confirmed by qRT-PCR.

Together, these findings suggest that PS-NH_2 triggers intracellular responses initiated at the membrane level, although the precise targets remain unidentified. Based on the DEGs, we propose the response mechanism illustrated in Fig. 6. The downregulation of *BAMBI*, an inhibitor of TGF-β signalling and a modulator of Wnt pathways [60, 61], may enhance TGF-β activity, leading to *TWIST1* upregulation, as previously observed [62]. TWIST1 can regulate *FOSL1*, a component of the AP-1 complex involved in inflammation, proliferation, and differentiation. FOSL1 overexpression has been associated with reduced cell adhesion and altered cell-cycle progression [63]. Our observation of *FOSL1* upregulation and increased expression of AP-1 downstream targets such as *S100A7* and *LCN2*, both implicated in inflammation and tumorigenesis [64, 65] supports this proposed mechanism.

Downregulation of *AXIN2* and *DKK4*, both negative regulators of Wnt/β-catenin signalling [66, 67], further suggests disruption of the Wnt pathway. Such disruption may promote β-catenin accumulation and nuclear translocation, activating targets like *FOSL1* and *CYP1A1* [68, 69] and amplifying inflammatory responses.

Taken together, PS-NH_2 NPs elicit a robust cellular response in Caco-2 cells involving TGF-β signalling, CYP induction, and Wnt pathway disruption. These results highlight a complex interplay of inflammation and stress-related pathways that may underlie the toxicity of functionalized nanoplastics in human intestinal epithelium. A key open question concerns the membrane receptor(s) recognized by PS-NH_2 NPs. As a speculative hypothesis, members of the Toll-like receptor family, particularly TLR4 and TLR2, may be involved, as they have been shown to recognize positively charged particles [70, 71]. Such interactions could activate NF-κB signalling, contributing to *BAMBI* downregulation and pro-inflammatory gene expression. This potential mechanism is included in Fig. 6 to guide future studies.

This transcriptomic approach allowed us to identify subtle yet biologically relevant alterations in stress and signalling pathways that may represent early indicators of long-term cellular adaptation or dysfunction, contributing to a mechanistic understanding essential for nanoplastic risk assessment. Further functional assays will be crucial to confirm the involvement of pathways such as TLR-mediated responses.

Conclusion

Fluorescent PS-COOH and PS-NH_2 NPs rapidly interacted with human intestinal Caco-2 cells, accumulating over 24 h. While PS-COOH were well tolerated, PS-NH2 showed higher toxicity. Transcriptomic analysis of PS-NH_2-exposed human intestinal Caco-2 cells has disclosed 125 differentially expressed genes (DEGs) with respect to control (untreated) cells, with 62 upregulated and 63 downregulated genes. Upregulated DEGs

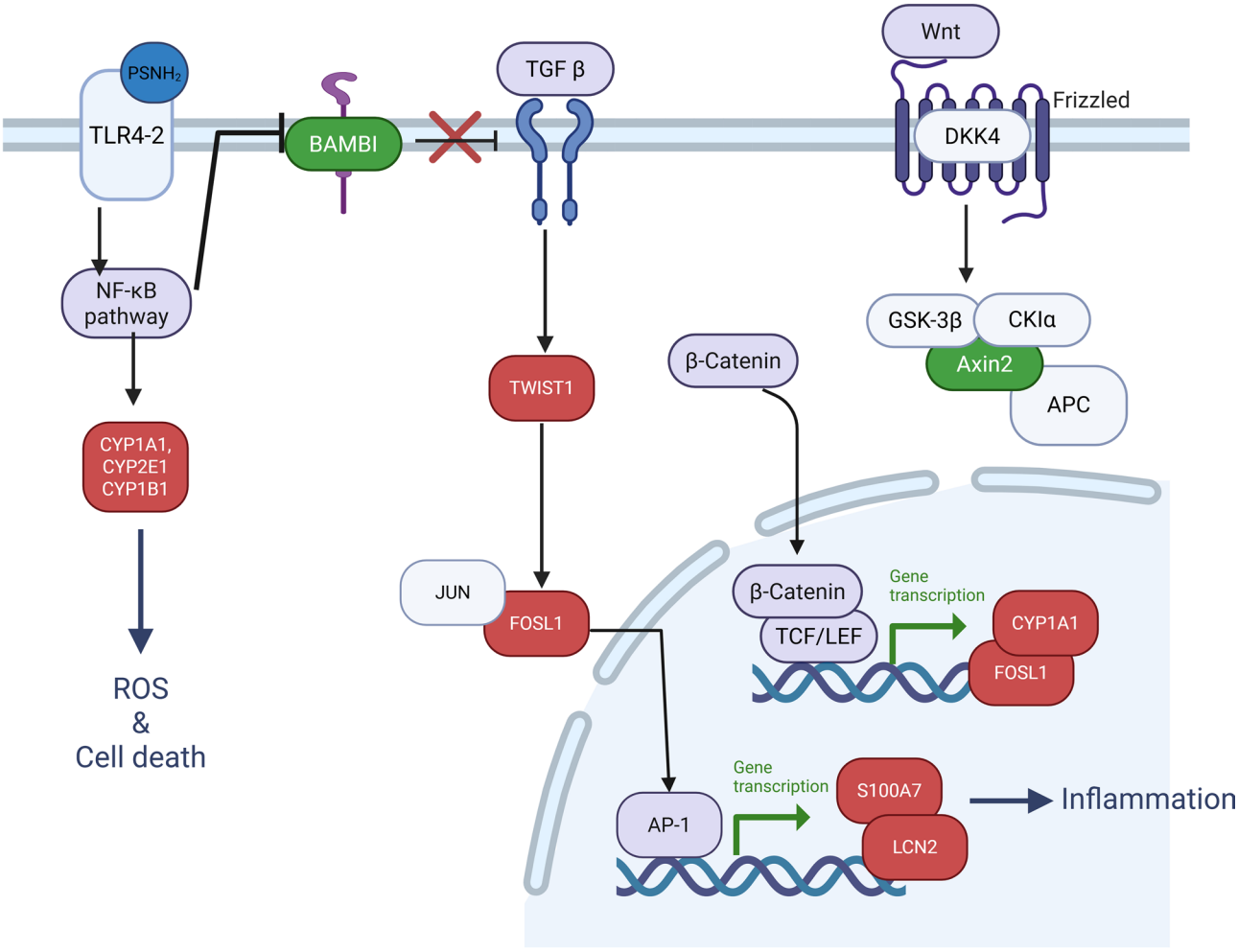

Fig. 6 Schematic representation of the hypothesized response of Caco-2 cells to PS-NH_2 exposure. The scheme is based on KEGG and GO analyses of differentially expressed genes and it integrates our experimental findings with proposed pathways to illustrate potential molecular targets and responses. Upregulated proteins are highlighted in red, downregulated proteins in green, and proteins expressed but not significantly altered are indicated in black. Toll-like receptors (TLR2 and TLR4) are included as putative membrane interaction sites, based on their reported ability to sense positively charged particles. Created in https://BioRender.com

included genes encoding cytochrome P450 enzymes (CYP1A1, CYP1A2, CYP1B1, CYP2E1) and aldehyde dehydrogenase 3 family member A1 (ALDH3A1). The KEGG pathway analysis revealed that these upregulated DEGs were highly associated with metabolism of xenobiotics by cytochrome P450 pathways. Other upregulated key genes were FOSL1, ADGRF1, and ZFP36, whereas AXIN2, ARRDC4, and the gene encoding Bone morphogenetic protein and activin membrane-bound inhibitor (BAMBI) were consistently downregulated. These expression changes were confirmed by qRT-PCR and were related to dysregulation of Wnt signalling pathway. Moreover, the upregulation of zinc finger protein 36 (ZFP36) gene, that encodes an RNA-binding protein promoting the decay of specific bound mRNA transcripts for inflammatory proteins [72]. indicates that NPs exposure can influence the expression of genes having critical roles in immune modulation. Thus, DEGs identified in PS-NH_2-treated cells were mainly linked to inflammation, detoxification of xenobiotics, oxidative stress, and suggest a dysregulation of Wnt signalling pathway. These findings highlight distinct cellular responses to functionalized PS NPs and offer insights into mitigating their impact on intestinal absorption.

Supplementary Information

The online version contains supplementary material available at https://doi.org/10.1186/s43591-025-00170-5.

Supplementary Material 1

Supplementary Material 2

Acknowledgements
We thank the School of Advanced Studies of the University of Camerino and the Fondazione Umberto Veronesi for the support respectively provided to Xueyan Liu and Junbiao Wang.

Author contributions
X.L.: conceived the study, conducted the investigation, developed the methodology, performed formal analysis, curated the data, generated the visualizations, and wrote the original draft; J.W.: conceived the study, conducted the investigation, developed the methodology, performed formal analysis, curated the data, and participated in manuscript review and editing; A.B.: conducted the investigation, developed the methodology, performed formal analysis, curated the data, generated the visualizations, and participated in manuscript review and editing; S.X.: conducted the investigation, developed the methodology, performed formal analysis, curated the data; D.P. and G.C.: provided resources, contributed to methodology development, participated in manuscript review and editing, and acquired funding; C.Ma.: conceived the study, provided resources, developed the methodology, participated in manuscript revision, acquired funding, and supervised younger researchers; C.Mi.: conceived the study, provided resources, developed the methodology, supervised younger researchers and coordinated manuscript review and editing. All authors read and approved the final manuscript and agreed to be held accountable for their contributions and the integrity of the work.

Funding
This study received funding from the European Union-Next-Generation UE-National Recovery and Resilience Plan (NRRP)-MISSION 4 COMPONENT 2, INVESTIMENT N. 1.1, CALL PRIN 2022 PNRR D.D. 1409 del 14-09-22 (Development of a biophotonic instrumentation to detect and quantify different types of microplastics present in aquatic ecosystems and evaluation of risks to human health (PlasticHealth)) CUP N. J53D23018540001.

Data availability
The datasets used and/or analysed during the current study, not included in this article and in its supplementary information files, are available from the corresponding authors on reasonable request. Reads from the transcriptomic study are deposited to NCBI Sequence Read Archive database, SRA accession: BioProject ID PRJNA1289666.

Declarations

Competing interests
The authors declare no competing interests.

Author details
[1]School of Biosciences and Veterinary Medicine, University of Camerino, Camerino 62032, Italy
[2]NanoDelivery Lab, Department of Molecular Medicine, Sapienza University of Rome, Viale Regina Elena 291, Rome 00161, Italy

Received: 18 September 2025 / Accepted: 17 December 2025
Published online: 25 December 2025

References

1. Wilcox C., Van Sebille E, Hardesty BD. Threat of plastic pollution to seabirds is global, pervasive, and increasing. Proc Natl Acad Sci. 2015;112:11899–904.
2. Nizzetto L, Langaas S, Futter M. Do microplastics spill on to farm soils? Nature. 2016;537:488.
3. Galloway TS, Lewis CN. Marine microplastics spell big problems for future generations. Proc Natl Acad Sci. 2016;113:2331–2333.
4. Bornscheuer UT. MICROBIOLOGY. Feeding on plastic. Science. 2016;351:1154–5.
5. Thompson RC, Olsen Y, Mitchell RP, Davis A, Rowland SJ, et al. Lost at sea: where is all the plastic? Science. 2004;304:838.
6. Cole M, Lindeque P, Halsband C, Galloway TS. Microplastics as contaminants in the marine environment: A review. Mar Pollut Bull. 2011;62:2588–97.
7. Song J, Wang C, Li G. Defining primary and secondary microplastics: A connotation analysis. ACS EST Water. 2024;4:2330–2.
8. Andrady AL, Barnes PW, Bornman JF, Gouin T, Madronich S, et al. Oxidation and fragmentation of plastics in a changing environment; from UV-radiation to biological degradation. Sci Total Environ. 2022;851:158022.
9. Cai L, Wang J, Peng J, Wu Z, Tan X. Observation of the degradation of three types of plastic pellets exposed to UV irradiation in three different environments. Sci Total Environ. 2018;628–629:740–7.
10. Gigault J, Halle AT, Baudrimont M, Pascal P-Y, Gauffre F, et al. Current opinion: what is a nanoplastic? Environ Pollut. 2018;235:1030–4.
11. Canesi L, Ciacci C, Bergami E, Monopoli MP, Dawson KA, et al. Evidence for Immunomodulation and apoptotic processes induced by cationic polystyrene nanoparticles in the hemocytes of the marine bivalve mytilus. Mar Environ Res. 2015;111:34–40.
12. Rist S, Baun A, Hartmann NB. Ingestion of micro- and nanoplastics in daphnia magna – Quantification of body burdens and assessment of feeding rates and reproduction. Environ Pollut. 2017;228:398–407.
13. Ma Y, Huang A, Cao S, Sun F, Wang L, et al. Effects of nanoplastics and microplastics on toxicity, bioaccumulation, and environmental fate of phenanthrene in fresh water. Environ Pollut. 2016;219:166–73.
14. Leslie HA, Velzen MJMV, Brandsma SH, Vethaak AD, Garcia-Vallejo JJ, et al. Discovery and quantification of plastic particle pollution in human blood. Environ Int. 2022;163:107199.
15. Amato-Lourenço LF, Carvalho-Oliveira R, Júnior GR, Dos Santos Galvão L, Ando RA, et al. Presence of airborne microplastics in human lung tissue. J Hazard Mater. 2021;416:126124.
16. Zhang C, Zhang G, Sun K, Ren J, Zhou J, et al. Association of mixed exposure to microplastics with sperm dysfunction: a multi-site study in China. eBioMedicine. 2024;108:105369.
17. Ragusa A, Svelato A, Santacroce C, Catalano P, Notarstefano V, et al. Plasticenta: First evidence of microplastics in human placenta. Environ. Int. 2021;146:106274.
18. Zhang J, Wang L, Trasande L, Kannan K. Occurrence of polyethylene terephthalate and polycarbonate microplastics in infant and adult feces. Environ Sci Technol Lett. 2021;8:989–94.
19. Ramsperger AFRM, Bergamaschi E, Panizzolo M, Fenoglio I, Barbero F, et al. Nano- and microplastics: a comprehensive review on their exposure routes, translocation, and fate in humans. NanoImpact. 2023;29:100441.
20. Sarkar AK, Rubin AE, Zucker I. Engineered Polystyrene-Based microplastics of high environmental relevance. Environ Sci Technol. 2021;55:10491–501.
21. Sadri SS, Thompson RC. On the quantity and composition of floating plastic debris entering and leaving the Tamar Estuary, Southwest England. Mar Pollut Bull. 2014;81:55–60.
22. Ziajahromi S, Neale PA, Rintoul L, Leusch FD. L. Wastewater treatment plants as a pathway for microplastics: development of a new approach to sample wastewater-based microplastics. Water Res. 2017;112:93–9.
23. Ren Z, Gui X, Xu X, Zhao L, Qiu H, et al. Microplastics in the soil-groundwater environment: Aging, migration, and co-transport of contaminants – A critical review. J Hazard Mater. 2021;419:126455.
24. Qiao J, Chen R, Wang M, Bai R, Cui X, et al. Perturbation of gut microbiota plays an important role in micro/nanoplastics-induced gut barrier dysfunction. Nanoscale. 2021;13:8806–16.
25. Jin Y, Xia J, Pan Z, Yang J, Wang W, et al. Polystyrene microplastics induce microbiota dysbiosis and inflammation in the gut of adult zebrafish. Environ Pollut. 2018;235:322–9.
26. Jin Y, Lu L, Tu W, Luo T, Fu Z. Impacts of polystyrene microplastic on the gut barrier, microbiota and metabolism of mice. Sci Total Environ. 2019;649:308–17.
27. Xu D, Ma Y, Han X, Chen Y. Systematic toxicity evaluation of polystyrene nanoplastics on mice and molecular mechanism investigation about their internalization into Caco-2 cells. J Hazard Mater. 2021;5:126092.
28. Saenen ND, Witters M, Hantoro I, Tejeda I, Ethirajan A, et al. Polystyrene microplastics of varying sizes and shapes induce distinct redox and mitochondrial stress responses in a Caco-2 monolayer. Antioxid Basel. 2023;12:739.
29. Zweibaum A, Hauri H-P, Sterchi E, Chantret I, Haffen K, et al. Immunohistological evidence, obtained with monoclonal antibodies, of small intestinal brush border hydrolases in human colon cancers and foetal colons. Int J Cancer. 1984;34:591–8.
30. Fogh J, Fogh JM, Orfeo T. One hundred and twenty-seven cultured human tumor cell lines producing tumors in nude mice. J Natl Cancer Inst. 1977;59:221–6.
31. Pinto M, Robine-Leon S, Appay M-D, Kedinger M, Triadou N, et al. Enterocyte-like differentiation and polarization of the human colon carcinoma cell line Caco-2 in culture. Biol Cell. 1983;47:323–30.

32. Marcellus KA, Prescott D, Scur M, Ross N, Gill SS. Exposure of polystyrene Nano- and microplastics in increasingly complex in vitro intestinal cell models. Nanomater Basel. 2025;15:267.
33. Lu L, Luo T, Zhao Y, Cai C, Fu Z, et al. Interaction between microplastics and microorganism as well as gut microbiota: A consideration on environmental animal and human health. Sci Total Environ. 2019;667:94–100.
34. Wu S, Wu M, Tian D, Qiu L, Li T. Effects of polystyrene microbeads on cytotoxicity and transcriptomic profiles in human Caco-2 cells. Env Toxicol. 2020;35:495–506.
35. Xiao S, Wang J, Digiacomo L, Amici A, Lorenzi VD, et al. Protein Corona alleviates adverse biological effects of nanoplastics in breast cancer cells. Nanoscale. 2024;16:16671–83.
36. Schindelin J, Arganda-Carreras I, Frise E, Kaynig V, Longair M, et al. Fiji: an open-source platform for biological-image analysis. Nat Methods. 2012;9:676–82.
37. Andrews S. FastQC: a quality control tool for high throughput sequence data. 2010. http://www.bioinformatics.babraham.ac.uk/projects/fastqc.
38. Love MI, Huber W, Anders S. Moderated Estimation of fold change and dispersion for RNA-seq data with DESeq2. Genome Biol. 2014;15:550.
39. Liao Y, Wang J, Jaehnig EJ, Shi Z, Zhang B. WebGestalt 2019: gene set analysis toolkit with revamped UIs and apis. Nucleic Acids Res. 2019;47:W199–205.
40. Piersanti A, Juganson K, Mozzicafreddo M, Wei W, Zhang J, et al. Transcriptomic responses to silver nanoparticles in the freshwater unicellular eukaryote tetrahymena thermophila. Env Pollut. 2021;269:115965.
41. Jeon S, Clavadetscher J, Lee D-K, Chankeshwara SV, Bradley M, et al. Surface Charge-Dependent cellular uptake of polystyrene nanoparticles. Nanomater Basel. 2018;8:1028.
42. Liu Y-Y, Liu J, Guo Y, Zhang Q, Cao A, et al. Interactions between polystyrene nanoparticles and human intestinal epithelial Caco-2 cells. NanoImpact. 2025;38:100559.
43. O'Connor A, Villalobos Santeli A, Nannu Shankar S, Shirkhani A, Baker TR, et al. Toxicity of microplastic fibers containing Azobenzene disperse dyes to human lung epithelial cells cultured at an air-liquid interface. J Hazard Mater. 2024;480:136280.
44. Zhao H, Ming T, Tang S, Ren S, Yang H, et al. Wnt signaling in colorectal cancer: pathogenic role and therapeutic target. Mol Cancer. 2022;21:144.
45. Khedri A, Guo S, Ramar V, Hudson B, Liu M. FOSL1's oncogene roles in Glioma/Glioma stem cells and tumorigenesis: A comprehensive review. Int J Mol Sci. 2024;25:5362.
46. Marques C, Unterkircher T, Kroon P, Oldrini B, Izzo A, et al. NF1 regulates mesenchymal glioblastoma plasticity and aggressiveness through the AP-1 transcription factor FOSL1. Elife. 2021;10:e64846.
47. Sääf AM, Halbleib JM, Chen X, Yuen ST, Leung SY, et al. Parallels between global transcriptional programs of polarizing Caco-2 intestinal epithelial cells in vitro and gene expression programs in normal colon and colon cancer. Mol Biol Cell. 2007;18:4245–60.
48. Fekete EE, Wang A, Creskey M, Cummings SE, Lavoie JR, et al. Multilevel proteomic profiling of colorectal adenocarcinoma Caco-2 cell differentiation to characterize an intestinal epithelial model. J Proteome Res. 2024;23:2561–75.
49. Proquin H, Jonkhout MCM, Jetten MJ, van Loveren H, de Kok TM, et al. Transcriptome changes in undifferentiated Caco-2 cells exposed to food-grade titanium dioxide (E171): contribution of the nano- and micro- sized particles. Sci Rep. 2019;9:18287.
50. Asif Mohyu Ali. Importance of polystyrene Nanoplastics, carboxyl Modifications, and their impacts on aquatic ecosystems. Org Chem Curr Res. 2023;12:349.
51. Kim E-H, Choi S, Kim D, Park HJ, Bian Y, et al. Amine-modified nanoplastics promote the procoagulant activation of isolated human red blood cells and thrombus formation in rats. Part Fibre Toxicol. 2022;19:60.
52. Yu Y, Xie D, Yang Y, Tan S, Li H, et al. Carboxyl-modified polystyrene microplastics induces neurotoxicity by affecting dopamine, glutamate, serotonin, and GABA neurotransmission in caenorhabditis elegans. J Hazard Mater. 2023;445:130543.
53. Forte M, Iachetta G, Tussellino M, Carotenuto R, Prisco M, et al. Polystyrene nanoparticles internalization in human gastric adenocarcinoma cells. Toxicol Vitro. 2016;31:126–36.
54. Zhang H, Cheng H, Wang Y, Duan Z, Cui W, et al. Influence of functional group modification on the toxicity of nanoplastics. Front Mar Sci. 2022;8-2021.
55. Schirinzi GF, Pérez-Pomeda I, Sanchís J, Rossini C, Farré M, et al. Cytotoxic effects of commonly used nanomaterials and microplastics on cerebral and epithelial human cells. Env Res. 2017;159:579–87.
56. Mokhosoev IM, Astakhov DV, Terentiev AA, Moldogazieva NT. Human Cytochrome P450 cancer-related metabolic activities and gene polymorphisms: a review. Cells. 2024;13:1958.
57. Bernkopf DB, Hadjihannas MV, Behrens J. Negative-feedback regulation of the Wnt pathway by conductin/axin2 involves insensitivity to upstream signalling. J Cell Sci. 2015;128:33–9.
58. Mozhgan A, Ranjbari J, Ghanbarian H. 7SK small nuclear RNA (Rn7SK) induces apoptosis through intrinsic and extrinsic pathways in human embryonic kidney cell line. Mol Biol Rep. 2024;51:96.
59. Tretina K, Park E-S, Maminska A, MacMicking JD. Interferon-induced guanylate-binding proteins: guardians of host defense in health and disease. J Exp Med. 2019;216:482–500.
60. Fritzmann J, Morkel M, Besser D, Budczies J, Kosel F, et al. A colorectal cancer expression profile that includes transforming growth factor inhibitor BAMBI predicts metastatic potential. Gastroenterology. 2009;137:165–75.
61. Liu K, Song X, Ma H, Liu L, Wen X, et al. Knockdown of BAMBI inhibits β-catenin and transforming growth factor β to suppress metastasis of gastric cancer cells. Mol Med Rep. 2014;10:874–80.
62. Celik-Turgut G, Olmez N, Koc T, Ozgun-Acar O, Semiz A, et al. Role of AHR, NF-kB and CYP1A1 crosstalk with the X protein of hepatitis B virus in hepatocellular carcinoma cells. Gene. 2023;853:147099.
63. Al-Khayyat W, Pirkkanen J, Dougherty J, Laframboise T, Dickinson N, et al. Overexpression of FRA1 (FOSL1) leads to global transcriptional Perturbations, reduced cellular adhesion and altered cell cycle progression. Cells. 2023;12:2344.
64. Cao S, Schnelzer A, Hannemann N, Schett G, Soulat D, et al. The transcription factor FRA-1/AP-1 controls Lipocalin-2 expression and inflammation in sepsis model. Front Immunol. 2021;12:701675.
65. Chu Y-W, Liu S-T, Cheng H-C, Huang S-M, Chang Y-L, et al. Opposing effects of Zac1 and Curcumin on AP-1-Regulated expressions of S100A7. PLoS ONE. 2015;10:e0144175.
66. Olsen AK, Coskun M, Bzorek M, Kristensen MH, Danielsen ET, et al. Regulation of APC and AXIN2 expression by intestinal tumor suppressor CDX2 in colon cancer cells. Carcinogenesis. 2013;34:1361–9.
67. Liu C, Chen X, Yang L, Kisseleva T, Brenner DA, et al. Transcriptional repression of the transforming growth factor β (TGF-β) pseudoreceptor BMP and activin Membrane-bound inhibitor (BAMBI) by nuclear factor κB (NF-κB) p50 enhances TGF-β signaling in hepatic stellate cells. J Biol Chem. 2014;289:7082–91.
68. Kasai S, Ishigaki T, Takumi R, Kamimura T, Kikuchi H. β-Catenin signaling induces CYP1A1 expression by disrupting adherens junctions in Caco-2 human colon carcinoma cells. Biochim Biophys Acta. 2013;1830:2509–16.
69. Schmidt S, Schumacher N, Schwarz J, Tangermann S, Kenner L, et al. ADAM17 is required for EGF-R-induced intestinal tumors via IL-6 trans-signaling. J Exp Med. 2018;215:1205–25.
70. Kedmi R, Ben-Arie N, Peer D. The systemic toxicity of positively charged lipid nanoparticles and the role of Toll-like receptor 4 in immune activation. Biomaterials. 2010;31:6867–75.
71. Park K-M, Kim B, Woo W, Kim LK, Hyun Y-M. Polystyrene microplastics induce activation and cell death of neutrophils through strong adherence and engulfment. J Hazard Mater. 2024;480:136100.
72. Cook ME, Bradstreet TR, Webber AM, Kim J, Santeford A, et al. The ZFP36 family of RNA binding proteins regulates homeostatic and autoreactive T cell responses. Sci Immunol. 2022;7:eabo0981.

Publisher's note